

# Geophysical Research Letters®

## RESEARCH LETTER

10.1029/2025GL115989

## Atmospheric Convection and Aerosol Absorption Boost Wildfire Smoke Injection

Rui Xu<sup>1</sup> , Yan Yu<sup>1,2</sup> , Xianglei Meng<sup>1</sup>, Huiwen Xue<sup>1,2</sup> , Chuanfeng Zhao<sup>1,2</sup> , and Jintai Lin<sup>1</sup> 

<sup>1</sup>Department of Atmospheric and Oceanic Sciences and Laboratory for Climate and Ocean-Atmosphere Studies, School of Physics, Peking University, Beijing, China, <sup>2</sup>China Meteorological Administration Tornado Key Laboratory, Beijing, China

### Key Points:

- Aerosol radiative absorption and atmospheric convection are incorporated into a smoke injection model
- The new parameterization accurately captures smoke height measured by space-borne lidar
- Pyrogenic factors and ambient convection lift smoke plumes by  $10^3$  and  $10^2$  m, respectively

### Supporting Information:

Supporting Information may be found in the online version of this article.

### Correspondence to:

Y. Yu,  
yuyan@pku.edu.cn

### Citation:

Xu, R., Yu, Y., Meng, X., Xue, H., Zhao, C., & Lin, J. (2025). Atmospheric convection and aerosol absorption boost wildfire smoke injection. *Geophysical Research Letters*, 52, e2025GL115989. <https://doi.org/10.1029/2025GL115989>

Received 15 MAR 2025

Accepted 9 JUL 2025

### Author Contributions:

**Conceptualization:** Rui Xu, Yan Yu

**Data curation:** Xianglei Meng

**Formal analysis:** Rui Xu, Yan Yu

**Methodology:** Rui Xu, Yan Yu, Huiwen Xue

**Validation:** Chuanfeng Zhao, Jintai Lin

**Visualization:** Rui Xu, Yan Yu

**Writing – original draft:** Rui Xu, Yan Yu

**Writing – review & editing:**

Xianglei Meng, Huiwen Xue,

Chuanfeng Zhao, Jintai Lin

**Abstract** Smoke released from increasingly severe wildfires has exerted widening impacts on the climate, ecosystem, and human life. Precisely quantifying these effects requires accurately representing smoke injection height in climate and air quality models. However, existing parameterizations of smoke injection height often diverge from actual observations, commonly underestimating smoke injection height from extreme burnings. In this study, we improve a widely used smoke injection model by integrating two critical processes: aerosol radiative absorption and atmospheric convection. The new parameterization, optimized and validated by satellite measurements of smoke extinction profiles above active fires, achieves a 10% reduction in root mean square error and an over 95% reduction in mean bias compared to its predecessor. Such improvements are especially pronounced in tropical and shrubland-dominated regions. This study underscores the critical role of aerosol self-lofting and convective processes in vertical dispersion of wildfire smoke, toward better quantifying its climate and environmental effects.

**Plain Language Summary** Wildfires release smoke plumes containing particles and gases into the atmosphere, impacting air quality, climate, and ecosystems. A key factor determining smoke's spatial dispersion and multifaceted impact is how high it rises from flames into the atmosphere; but current smoke injection models often fail to match real-world observations, especially for those extremely elevated plumes. This study introduces a new smoke injection model that incorporates two critical processes: the absorption of sunlight by black carbon and the energy from atmospheric convection. Using satellite data and meteorological reanalysis, we optimize and validate the model, which substantially outperforms its predecessor in estimating smoke plume heights. The model reduces root mean square error by over 10% and improves accuracy for extreme smoke injection events, especially in tropical and shrubland-dominated regions. By accounting for additional smoke rising forces from atmospheric convection and aerosol absorption, the new model accurately captures the extreme smoke injections and provides a stronger foundation for quantifying the long-range transport and environmental impacts of wildfire emissions.

## 1. Introduction

Wildfire smokes play a critical role in the Earth system, influencing air quality, climate and ecosystem dynamics on a global scale. Emissions from wildfires are a major source of trace gases and aerosols in the atmosphere, significantly affecting air quality and posing risks to human health (Bourgeois et al., 2021; Koning et al., 1985). These aerosols also alter the radiative budget (Heinold et al., 2022), thereby influencing climate variations such as tropical Pacific cooling (Fasullo et al., 2023) and contributing to severe convective storms (Zhang et al., 2019). Beyond atmospheric effects, wildfire aerosols also affect terrestrial and oceanic nutrient cycles, underscoring their importance in the entire Earth system (Hamilton et al., 2022; Li et al., 2021).

The maximum altitude to which a wildfire plume is injected from the active flame, referred to as the wildfire smoke injection height, along with the vertical distribution of aerosols and gases are key parameters for describing the atmospheric dispersion of wildfire smoke. These parameters are also essential inputs for climate and air quality models that aim to simulate the environmental effects of wildfire smoke. In particular, past studies have demonstrated the key role of smoke injection height in the residence time of aerosols in the atmosphere, the extent of their long-range transport, and ultimately their environmental and climatic impacts (Kahn et al., 2007; Labonne et al., 2007; Val Martin et al., 2018).

Current climate models often rely on empirical estimates to simulate wildfire smoke injection heights, typically assuming a uniform vertical distribution from the surface to a predetermined height based on general factors. For

© 2025. The Author(s).

This is an open access article under the terms of the [Creative Commons Attribution License](https://creativecommons.org/licenses/by/4.0/), which permits use, distribution and reproduction in any medium, provided the original work is properly cited.

instance, models participating in the Aerosol Inter Comparison Project Phase I (AeroCom-I) assigned fixed smoke heights for a specific latitude and landcover (Dentener et al., 2006). While some models set smoke top heights at approximately 2 km (Davison et al., 2004), others, such as those focusing on Canadian wildfires, estimate heights between 5 and 8 km (Westphal & Toon, 2012). However, actual smoke emission and distribution depend heavily on wildfire intensity and concurrent meteorological conditions.

To improve model's simulations of wildfire smoke, dynamical smoke height models have been introduced. Freitas et al. combined 1-D plume uplift with a 3-D dispersion to propose a dynamic smoke height model (Freitas et al., 2007, 2010). Although this model has been refined and integrated into various climate models to study wildfire smoke effects (Lu et al., 2023; Ma et al., 2024), it remains computationally intensive due to its reliance on solving differential equations for individual wildfire events. Alternatively, Sofiev et al. (2012) developed a semi-empirical model based on energy balance during plume ascent. It achieved high accuracy with largely reduced computational burden, but exhibited its own limitations. Specifically, the Sofiev model described vertical uplift only due to initial energy release from burning, planetary boundary layer height, and free tropospheric stability, while excluding other potentially influential processes. Additionally, the model parameters were estimated using spatio-temporally limited satellite data. These limitations caused an insufficient capability of the Sofiev model in capturing the extremely high injection of smoke plumes (Paugam et al., 2016; Sofiev et al., 2012). Subsequent applications of the Sofiev's smoke injection height model, in either observational diagnosis or numerical simulations (Li et al., 2023; Sofiev et al., 2013; Veira et al., 2015), raised concerns about these uncertainties.

Recent case studies revealed additional processes that influence smoke injection heights. For example, de Laat et al. (2012) first identified the smoke self-lofting driven by aerosol absorption of solar radiation during the 2009 Australian Black Saturday event, followed by studies demonstrating such self-lofting being responsible for transporting smoke aerosols into the stratosphere (Khaykin et al., 2020; Ohneiser et al., 2023; Yu et al., 2019). Concurrently, pyrocumulonimbus (pyroCb) events—extreme convective process triggered by wildfires—have been increasingly observed. Under appropriate meteorological conditions, pyroCb can rapidly inject large volumes of smoke to the tropopause or even the stratosphere, facilitating long-range transport and influencing both tropospheric and stratospheric environments (Peterson et al., 2018, 2021; Rodriguez et al., 2020; Rosenfeld et al., 2007). Analogous to pyroCb events, ambient atmospheric convection could also lift smoke plumes to higher altitudes. Nevertheless, despite their apparent contribution to extremely elevated smoke plumes, radiative absorption and convection have not been adequately represented in existing semi-empirical models like the Sofiev model.

Here we integrate the previously reported two critical processes: aerosol radiative absorption and atmospheric convection, to improve the smoke injection height model developed by Sofiev et al. (2012). This model balances theoretical rigor with computational efficiency, and is optimized with aerosol profiles measured by space-borne lidar.

## 2. Materials and Methods

### 2.1. Satellite-Based Identification of Smoke Injection Height

We first retrieve smoke injection height from aerosol vertical profiles measured by Cloud-Aerosol Lidar with Orthogonal Polarization (CALIOP) aboard CALIPSO satellite (Kim et al., 2018; Powell et al., 2009). To collocate with other data used here, three-dimensional samples of extinction coefficient labeled by “smoke” and “elevated smoke” aerosols are obtained from the CALIOP Level 2 Vertical Feature Mask product (VFM) and 532-nm Aerosol Profile products (version 4.51), horizontally aggregated to  $0.1^\circ \times 0.1^\circ$  grids, and vertically retained at their original resolution.

We subsequently apply wavelet covariance transform method (WCT) (Huang et al., 2024; Michailidis et al., 2021) to the gridded smoke extinction coefficient profiles to determine the smoke injection heights. The WCT function is defined as

$$W_f(a, b) = \frac{1}{a} \int_{z_b}^{z_t} f(z) h\left(\frac{z-b}{z}\right) dz, \quad (1)$$

where  $z_b$  and  $z_t$  represent the bottom and top height of the profile respectively,  $f(z)$  is profile function and  $h(z)$  is the Haar wavelet, and parameter  $a$  is 30 times the vertical resolution. Smoke extinction coefficient profiles with a smoke bottom height exceeding 150 m above ground, indicative of a non-local source, or over 40% missing values are excluded. The uppermost positive peak of WCT profile exceeding the threshold value 0.04 is defined as the smoke plume top and its corresponding altitude is defined as the injection height.

To identify wildfire locations and obtain fire intensity, the Moderate Resolution Imaging Spectroradiometer (MODIS) active fire and Fire Radiative Power (FRP) products (Giglio et al., 2016) are utilized. MODIS is an instrument aboard the Terra and Aqua satellites, crossing the equator at around 10:30 a.m. local time (LT) and 1:30 p.m. LT, respectively. Since the afternoon overpass is closer to that of CALIPSO, only Aqua MODIS data is used in the following analysis. Similar to the processing of CALIOP data, MODIS FRP is also aggregated by  $0.1^\circ \times 0.1^\circ$  grids.

Next we collocate CALIOP and MODIS measurements to establish an observational inventory of wildfire smoke injection height. When CALIOP captures a valid smoke extinction profile within  $0.2^\circ$  of any  $0.1^\circ$  grid that contains valid MODIS FRP, the smoke extinction coefficient profiles within the  $1^\circ \times 1^\circ$  grids centered on the active fire point are horizontally averaged to obtain a spatially complete, vertical distribution of smoke aerosols. This approach identifies 60,306 global smoke plumes captured by CALIOP for the periods 2008–2018. Afterward, the abovementioned WCT method is applied to the average profile to calculate the smoke injection height.

## 2.2. Improving the Semi-Empirical Model for Smoke Injection Height

Our work is based on the simple model derived by Sofiev et al. (2012) of the form

$$H_p = \alpha H_{abl} + \beta \left( \frac{FRP}{P_{f0}} \right)^\gamma \exp \left( -\delta \frac{N_{FT}^2}{N_0^2} \right), \quad (2)$$

where

$$\alpha = 0.24, \beta = 170 \text{ m}, \gamma = 0.35, \delta = 0.6. \quad (3)$$

here,  $H_{abl}$  represents the atmospheric boundary layer height; FRP characterizes the energy released by wildfire combustion;  $N_{FT}$  is the Brunt–Väisälä frequency at twice the boundary layer height, used to characterize the stability of the atmospheric layer below;  $P_{f0} = 1 \times 10^6 \text{ W}$ ,  $N_0^2 = 2.5 \times 10^{-4} \text{ s}^{-2}$  are two given empirical constants. The parameters in Equation 3 were determined from the loss function

$$J_R = \sum_{i=1}^{N_{\text{fires}}} \Theta(|H_p^{\text{obs}}(i) - H_p^{\text{mdl}}(i)| - \Delta h), \quad (4)$$

$$\Theta(x) = \begin{cases} 0, & x \leq 0 \\ 1, & x > 0 \end{cases},$$

where  $H_p^{\text{obs}}$  was the stereo height of North American and Siberian plumes ( $N_{\text{fires}} = \sim 2,000$ ) during the 2007–2008 fire seasons, measured by the Multi-angle Imaging SpectroRadiometer (MISR) instrument and retrieved by the MISR Interactive eXplorer (MINX) software (Nelson et al., 2013);  $\Delta h$  was the observational error (500 m) (Val Martin et al., 2018) of MISR stereo height.

To demonstrate the accuracy of Sofiev model in capturing the CALIOP-based smoke height, we optimize the parameters by minimizing the original loss function (Equation 4) with  $H_p^{\text{obs}}$  from CALIOP-based height and  $\Delta h$  of 150 m (5 times CALIOP vertical resolution). The optimization results in updated parameters of

$$\alpha = 0.86, \beta = 100.2 \text{ m}, \gamma = 0.25, \delta = 0.49, \quad (5)$$

with  $P_{f0}$  adjusted to  $5 \times 10^5$  W. Using these updated parameters, this set of calculated heights provides the benchmark for evaluating the model performance improvements by introducing an alternative loss function and additional processes.

To develop an improved model, firstly, we use Root Mean Square Error (RMSE) as the new loss function. The original loss function counted predictions outside the observational error range. However, it treated all fire events equally, without measuring specific errors; so extreme errors, often associated with extremely elevated plumes, were not accounted for in the model. In addition, here we use CALIOP-based smoke height, which is better capable of identifying diluted smoke edges than MISR as used in Sofiev et al. (2012) (Huang et al., 2024; Nelson et al., 2013; Paugam et al., 2016; Tosca et al., 2011). Therefore, here we choose RMSE as the loss function, formulated as

$$\text{RMSE} = \sqrt{\frac{\sum_{i=1}^{N_{\text{fires}}} (H_p^{\text{obs}}(i) - H_p^{\text{mdl}}(i))^2}{N_{\text{fires}}}} \quad (6)$$

Subsequently, two additional physical processes that may enhance the lifting of smoke are considered. The first is the radiative absorption by emitted aerosols, represented here by aerosol optical depth of black carbon ( $\text{AOD}_{\text{BC}}$ ), since BC is the primary absorbing aerosol in smoke. Given that the aerosol absorption effect supplies additional energy for smoke lifting,  $\text{AOD}_{\text{BC}}$  is included following the FRP term, modifying the model formula to

$$H_p = \alpha H_{\text{abl}} + \beta \left( \frac{\text{FRP}}{P_{f0}} + \varepsilon \frac{\text{AOD}_{\text{BC}}}{\tau_0} \right)^\gamma \exp\left(-\delta \frac{N_{\text{FT}}^2}{N_0^2}\right), \quad (7)$$

The second process is atmospheric convection. To quantify the potential for convection, convective available potential energy (CAPE) is used as an indicator of atmospheric instability. While both CAPE and the Brunt–Väisälä frequency can describe atmospheric instability, the latter only accounts for the influence of the potential temperature profile, whereas CAPE considers humidity additionally. And since CAPE also quantifies the additional energy provided for smoke lifting during convection, it is incorporated into the model as a factor following the FRP term, replacing the Brunt–Väisälä frequency term, as

$$H_p = \alpha H_{\text{abl}} + \beta \left( \frac{\text{FRP}}{P_{f0}} + \varepsilon \frac{\text{AOD}_{\text{BC}}}{\tau_0} + \omega \frac{\text{CAPE}}{E_0} \right)^\gamma, \quad (8)$$

with  $\tau_0 = 0.001$  and  $E_0 = 500 \text{ J kg}^{-1}$ .

To more accurately account for convection effects, a “two-step” model is developed based on Equation 8. Convective available potential energy, by definition, influences the lifting of air parcels only when they reach the level of free convection (LFC). Therefore, the “two-step” model is structured as follows: first, a preliminary height  $H_{\text{detect}}$  is calculated. If  $H_{\text{detect}}$  exceeds the LFC, CAPE is introduced in the calculation following Equation 8; otherwise, CAPE is excluded and the injection height is calculated following Equation 7.  $H_{\text{detect}}$  is calculated by using Equation 8, with RMSE loss function—replacing  $H_p^{\text{mdl}}(i)$  by  $H_{\text{detect}}(i)$  in Equation 5—for parameter fitting. To better characterize the wildfire smoke capable of exceeding the LFC, smoke heights higher than the 75th percentile in the current inventory are used as the training set for  $H_{\text{detect}}$ .

In summary, the improved smoke injection height model is a “two-step” model (Figure 1). Parameters for this model are derived from minimizing RMSE against CALIOP-observed smoke heights from CALIOP, using a randomly selected 80% of observational data as the training set.

### 2.3. Data From ERA5 and EAC4

This study employs the European Center for Medium-Range Weather Forecasts (ECMWF) Reanalysis v5 (ERA5) global reanalysis data set, specifically utilizing hourly temperature, geopotential, and relative humidity at pressure levels, as well as boundary layer height and CAPE at single levels (Hersbach et al., 2023a, 2023b). The data set is provided at a horizontal resolution of  $0.25^\circ \times 0.25^\circ$ , covering 1950 to present. In our work, boundary

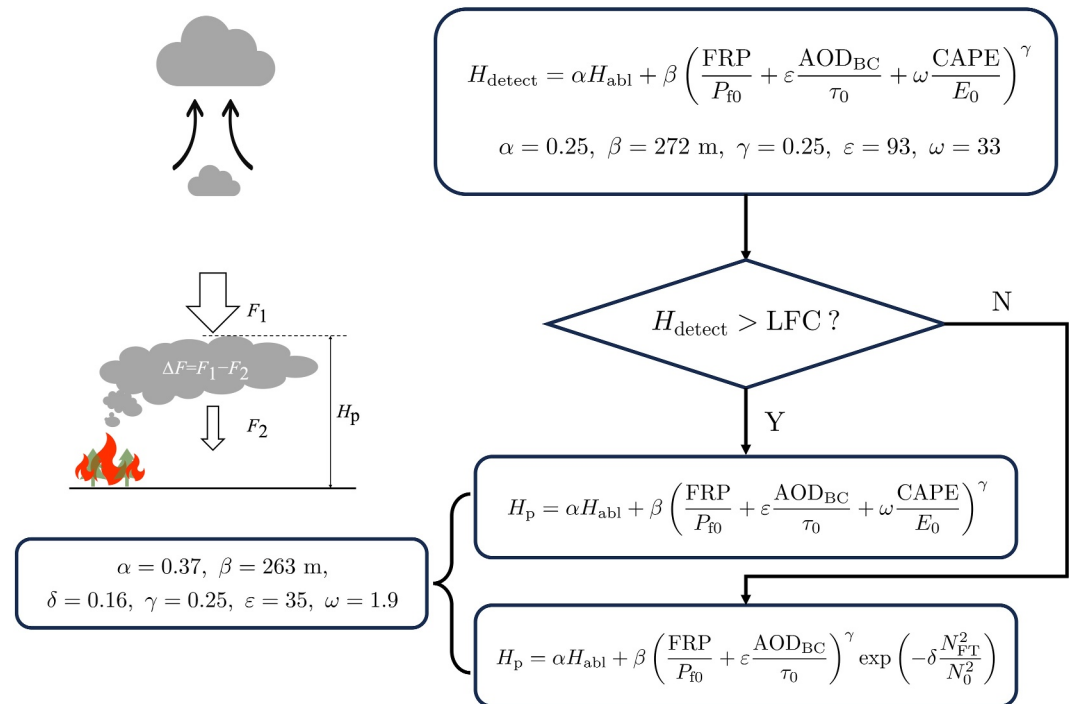


**Figure 1.** Flowchart of model development demonstrating the model structure and optimized value of the parameters.

layer height and CAPE are directly integrated into the smoke injection height model, while temperature, geopotential, and relative humidity data are utilized in the computation of LFC.

The black carbon aerosol optical depth at 550 nm ( $\text{AOD}_{\text{BC}}$ ) used in the improved model is sourced from the ECMWF Atmospheric Composition Reanalysis 4 (EAC4). EAC4 assimilates modeled and observed atmospheric composition globally (Inness et al., 2019). In particular, wildfire emissions based on MODIS FRP are estimated by the Copernicus Atmosphere Monitoring Service (CAMS) Global Fire Assimilation System (Kaiser et al., 2012) and used for subsequent simulation of all species including  $\text{AOD}_{\text{BC}}$ . EAC4 provides 3-hourly  $\text{AOD}_{\text{BC}}$  for the period from 2003 to present with a  $0.75^\circ \times 0.75^\circ$  horizontal resolution.

The average value of the meteorological field and the maximum value of boundary layer height, CAPE and  $\text{AOD}_{\text{BC}}$  within  $1^\circ \times 1^\circ$  near the fire point are substituted into calculation.

### 3. Results

#### 3.1. Improved Accuracy of the New Smoke Injection Height Model

The observational smoke injection heights (Figure 2a), detected from CALIOP and retrieved using the algorithm outlined in Section 2.1, capture the global distribution of smoke injection height, similar to MISR stereo height as widely analyzed in previous studies (Kahn et al., 2007; Paugam et al., 2016; Val Martin et al., 2010) but with generally greater values (Figure S1 in Supporting Information S1). The maximum observed height exceeds 6,000 m a.m.s.l (Figure 2a), indicating that CALIOP, despite its sparse coverage, is able to pick up extreme wildfire events with high injections. Elevated smoke injections are primarily observed in the tropics of Africa and Asia, while a smaller proportion is detected over North America. Possible reasons for greater smoke heights in CALIOP than in MISR are: (a) CALIOP measures daytime aerosols at about 1:30 p.m. LT, three hours later than MISR, thus allowing for further development of smoke plumes especially with afternoon atmospheric convection, and (b) CALIOP is more capable than the MISR stereo product at detecting optically thin aerosol layers, such as those found over the top edges of smoke (Figure S1c in Supporting Information S1).

The new two-step model achieves minor bias reduction by adopting RMSE as the loss function and major improvements by incorporating  $\text{AOD}_{\text{BC}}$  and CAPE, against the original Sofiev model (Figure 2). A comparison

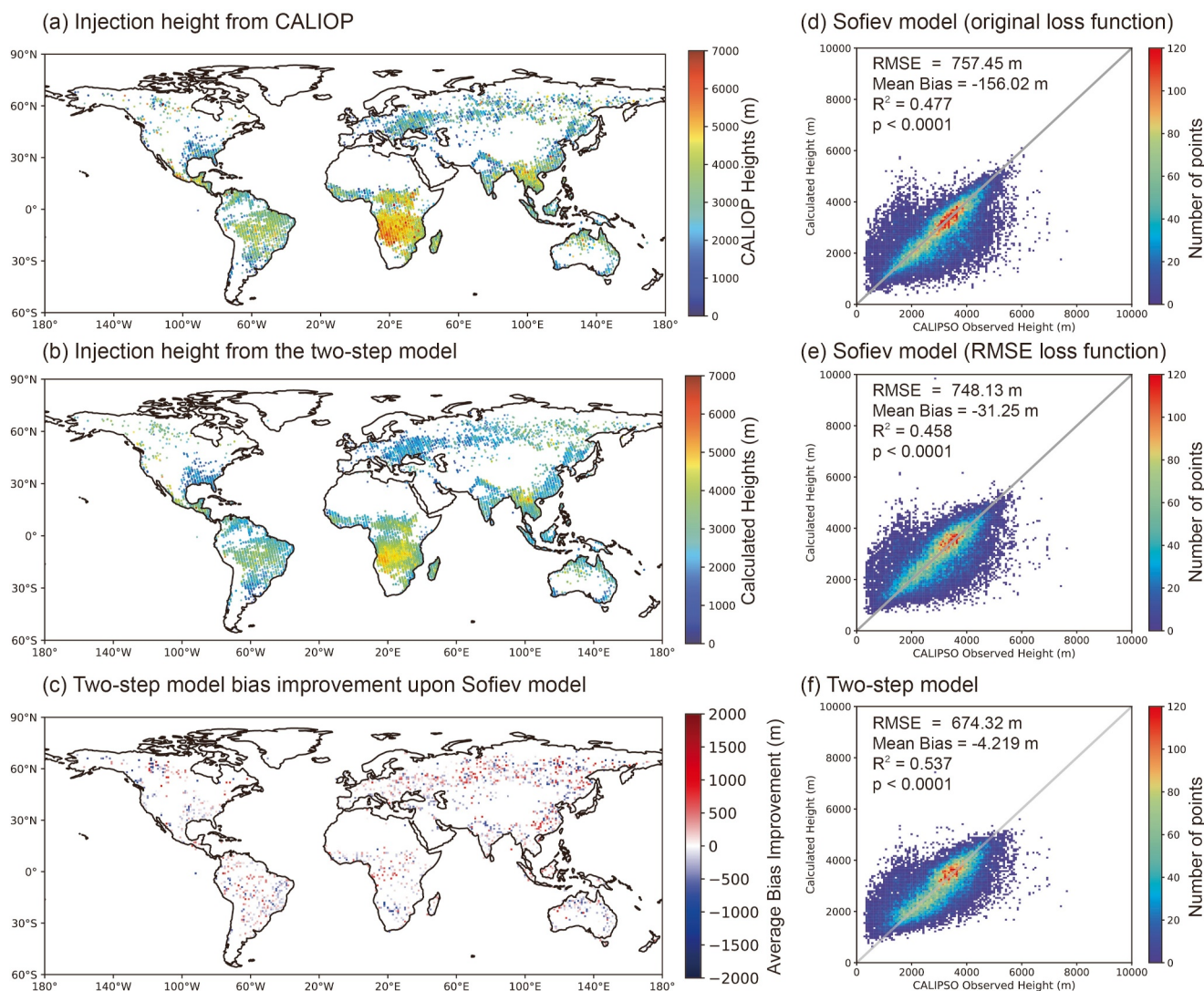


**Figure 2.** Observed and simulated smoke injection heights. (a) CALIOP-observed smoke injection heights (meters above mean sea level, m a.s.l.). (b) Calculated heights from the two-step model (m a.s.l.). (c) Bias reduction from the Sofiev model optimized using CALIOP-based heights and Equation 4 to the new two-step model. The bias reduction is quantified as the difference of the absolute biases between the two models. Results are averaged over  $1^\circ \times 1^\circ$  global grids, with only grids showing consistent bias changes (increase or decrease) in over 90% of cases being displayed. (d–f) Joint probability density functions of observed versus simulated smoke injection heights from (d) Sofiev model optimized using the (d) original and (e) RMSE-based loss functions, and (f) two-step model. These results are derived from the full data set, encompassing both training and testing sets.

between the Sofiev model optimized using the original and RMSE-based loss function indicates improved simulation in the high injection cases especially those exceeding 4,000 m and an average bias reduction over 100 m by the RMSE-based Sofiev model (Figures 2d and 2e). Compared with the RMSE-based Sofiev model (Figure 2e), the two-step model (Figure 2f) achieves further skills, evidently diminishing the overestimation for smoke injection heights below 2,000 m and underestimation for smoke heights above 3,000 m (Figure 2f). Notable bias reduction exceeding 1,500 m are observed in the tropical South America, Africa, and Asia, as well as in the boreal Eurasia and North America (Figure 2c). Additional sensitivity tests indicate a reduction in RMSE and mean bias by 65 and 33 m, respectively, introduced by  $AOD_{BC}$ ; whereas CAPE causes 48 and 227 m reductions in these error metrics (Table S1 in Supporting Information S1).

Such improvements by incorporating  $AOD_{BC}$  and CAPE in the two-step model are particularly evident in extreme smoke injection events in which aerosol absorption and ambient convection have been reported as key factors lifting the smoke plumes (Figure 3). In the August 2010 Brazilian fires, the CALIOP measurements indicate widespread smoke plumes rising to about 4,000 m (Gonzalez-Alonso et al., 2019), partially attributable to the

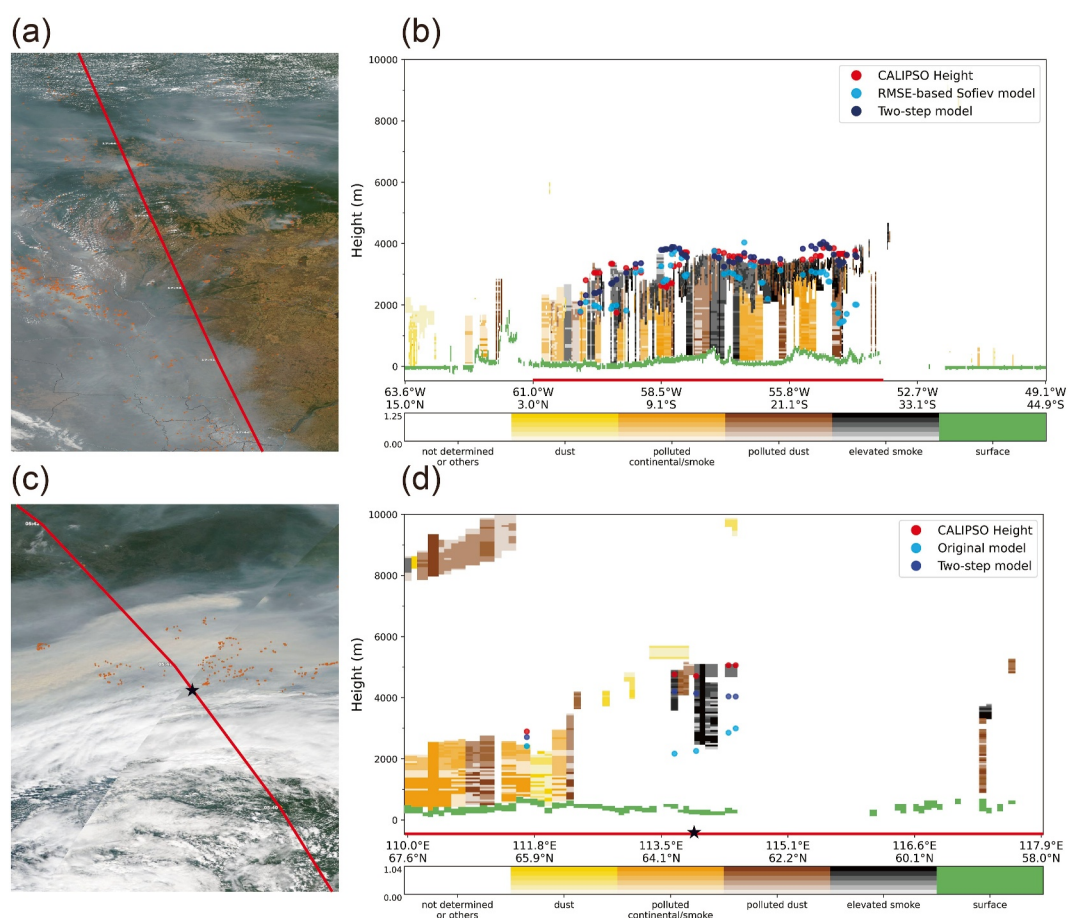


**Figure 3.** Improved accuracy of the two-step model against the RMSE-based Sofiev model during (a, b) Brazil fires on 25 August 2010, and (c, d) Central Siberian fires on 5 August 2021. (a, c) Aqua Moderate Resolution Imaging Spectroradiometer (MODIS) true color image overlaid by Aqua MODIS daytime fire spots (orange points) and CALIPSO Orbit Track (red line). (b, d) Profiles of aerosol type along the CALIPSO track from the Cloud-Aerosol Lidar with Orthogonal Polarization VFM product, with the extinction coefficient indicated by transparency of the colorblocks. Red, blue, and indigo dots indicate the CALIPSO-observed, Sofiev model-simulated, and two-step model-simulated heights, respectively. The red lines on the x-axis of (b, d) correspond to the track in (a, c). The star on the x-axis of (d) corresponds to the same marker in (c).

abundant CAPE exceeding  $1204 \text{ J kg}^{-1}$ . While the RMSE-based Sofiev model underestimates the injection height by about 500 m, the new two-step model well captures these elevated smoke plumes (Figure 3b). Similarly, the two-step model reproduces the smoke height at about 5,000 m during the August 2021 Central Siberian fires (Figures 3c and 3d), in which a smoke layer with  $\text{AOD}_{\text{BC}}$  of  $\sim 0.1$  introduced an additional lofting velocity of  $\sim 1.5 \text{ km day}^{-1}$  in the lower troposphere (Ohneiser et al., 2023).

### 3.2. Contribution of Pyrogenic Factors and Ambient Convection to Smoke Injection Height

Sensitivity tests are conducted to quantify the contribution of pyrogenic factors, namely FRP and  $\text{AOD}_{\text{BC}}$ , and CAPE in the simulated smoke injection heights (Figure 4). The aggregated influence of FRP and  $\text{AOD}_{\text{BC}}$  widely exceeds 1,500 m in both the tropics and mid-to-high latitudes (Figure 4a). Different land cover types see generally  $\sim 10^3 \text{ m}$  of smoke lifting caused by pyrogenic thermal and radiative effects, with slightly greater contributions in shrubland-dominated areas (Figure 4b). In contrast, the impact of CAPE is predominantly concentrated in tropical regions ( $30^\circ\text{S}$ – $30^\circ\text{N}$ ), where over 8% of cases see a nontrivial contribution of CAPE, in contrast to 4% of nontrivial CAPE contribution in the extratropics (Figure 4d). Effects of CAPE are particularly evident in the equatorial regions, where CAPE causes an extra smoke ascent by over 500 m (Figure 4c). This pattern aligns with the higher likelihood of strong convective activity occurring in tropical regions. Quantitatively, CAPE contributes

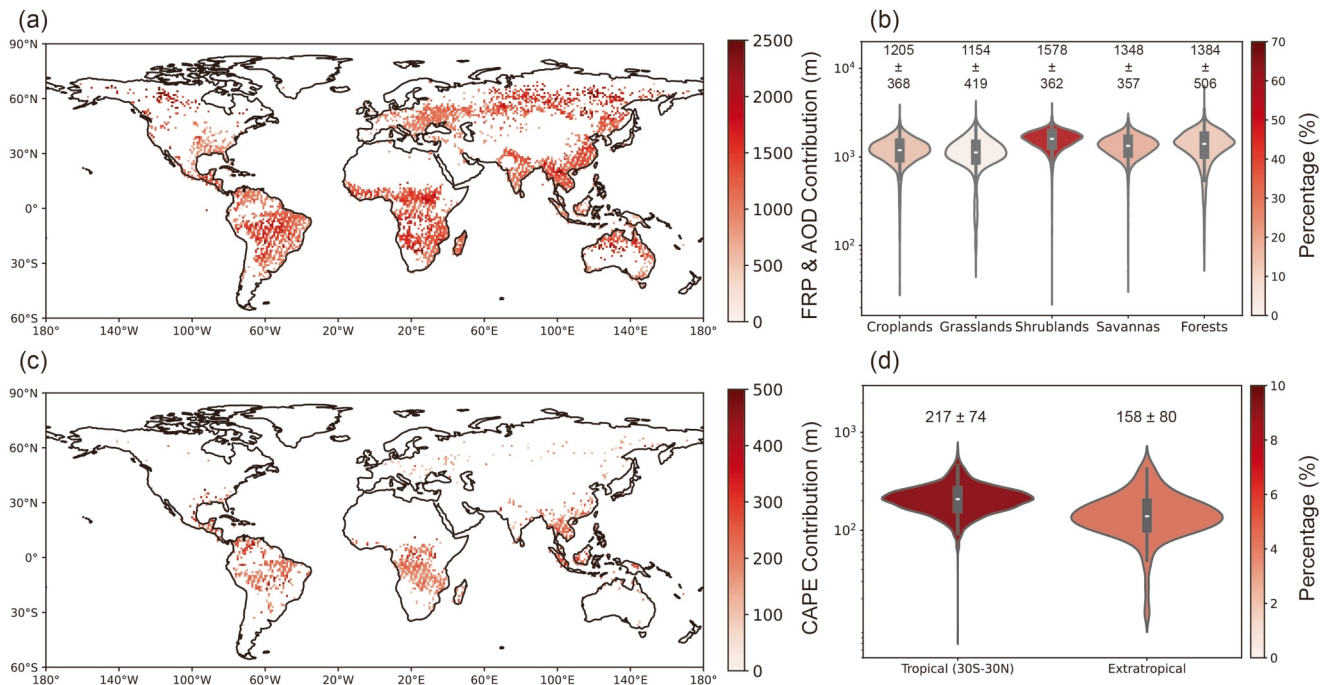


**Figure 4.** Sensitivity of smoke injection height to pyrogenic factors (Fire Radiative Power (FRP) and AOD<sub>BC</sub>) and convective available potential energy (CAPE) as simulated by the new two-step smoke injection model. (a) Map showing the difference in simulated smoke height between using the actual FRP and AOD<sub>BC</sub> and using zero for both variables. (b) Violin plots of the results in (a) for croplands, grasslands, shrublands, savannas and forests, with color indicating the proportion of all cases falling into each land cover type; numbers represent the average and standard deviation in black carbon's contribution to smoke injection (m) among cases for each land cover type; (c) As in (a), but for the CAPE term. (d) Violin plots of the results in (c) tropical (30°S–30°N) and extratropical regions in which CAPE makes a nontrivial contribution to the injection height. The color of the violins in (d) indicate the percentage of cases where CAPE makes a nontrivial contribution.

~10<sup>2</sup> m of additional smoke lifting, with an average ( $\pm$  standard deviation) contribution of 217 ( $\pm$ 74) m in the tropics and a wider range of contribution at 158 ( $\pm$ 80) m in the extratropics (Figure 4d).

#### 4. Conclusion and Discussion

On the basis of Sofiev smoke injection model, here we introduce two additional processes: aerosol radiation absorption and atmospheric convection, and optimize the parameterization by minimizing the RMSE against CALIOP-based smoke injection height. Compared to the original model, our new “two-step” model achieves a 10% reduction in RMSE and over 95% decrease in mean bias. The extreme smoke injection cases and sensitivity experiments demonstrate the substantial impacts of black carbon and CAPE on the accuracy of smoke injection height simulations. The new two-step model developed in this study could be applied directly in smoke height diagnosis and potentially useful in Earth System modeling. Based on sensitivity experiments within the two-step model, pyrogenic factors, namely fire radiative and thermodynamic effects, and ambient convection lift smoke plumes by  $\sim$ 10<sup>3</sup> and  $\sim$ 10<sup>2</sup> m, respectively.

Despite the significant advancements of the two-step smoke injection height model, several sources of uncertainty remain in the present study. First, the currently analyzed satellite data collection provides a spatio-temporally insufficient sample of smoke injection height. Although CALIOP has better sensitivity to optically thin smoke layers compared with MISR, its narrow horizontal footprint (Powell et al., 2009) leads to limited sampling, especially underrepresenting the relatively rare, extreme smoke lifting events. Meanwhile, the currently analyzed polar-orbiting satellite instruments, namely MODIS and CALIOP, only present snapshots of wildfires and associated smoke, leading to vague time scales of the smoke development and possible mismatch between the CALIOP-observed smoke plume and MODIS-observed FRP within the currently analyzed 1° pixels. Although our additional test of restricting the collocation to 0.5° pixels shows generally consistent smoke heights with that in 1° pixels (Figure S2 in Supporting Information S1), possible extension of spatial and temporal coverage of CALIOP-like measurements will unfold a dynamical picture of smoke injection processes. Second, the current formulation using AOD<sub>BC</sub> is applicable for diagnosing smoke injection height from satellite data but

inappropriate for chemical transport or climate models, which usually simulate  $AOD_{BC}$  using injection height as an input. We choose  $AOD_{BC}$  due to the dependence of BC emission on FRP in currently available data sets; such collinearity prohibits an assessment of their respective contribution to smoke lifting. Yet, the currently adopted  $AOD_{BC}$  also partially depends on FRP, preventing a definite evaluation of BC-induced self-lifting. Future improvements and expanded application of the smoke injection model will benefit from spatio-temporally continuous monitoring of smoke injection process along with accurate aerosol emission quantification.

Our results emphasize the intricate interactions between black carbon emission, ambient convection, and smoke injection heights. For example, intensified convection not only promotes higher smoke injections but also serves as a precursor for lightning ignition and low-level oxygen convergence (Su et al., 2025). These multi-way influences of convection suggest a possibly promoted smoke height injected from the increasingly stronger extratropical forest fires with stronger convection under global warming (Janssen et al., 2023; Meng et al., 2025).

### Data Availability Statement

The ERA5 data on pressure level and single level are available through (Hersbach et al., 2023a) (<https://doi.org/10.24381/cds.bd0915c6>) and (Hersbach et al., 2023b) (<https://doi.org/10.24381/cds.adbb2d47>), respectively. The CALIOP Level 2 Vertical Feature Mask product is available through (NASA/LARC/SD/ASDC, 2022b) ([https://doi.org/10.5067/CALIOP/CALIPSO/CAL\\_LID\\_L2\\_VFM-Standard-V4-51](https://doi.org/10.5067/CALIOP/CALIPSO/CAL_LID_L2_VFM-Standard-V4-51)) and Aerosol Profile product is available through (NASA/LARC/SD/ASDC, 2022a) ([https://doi.org/10.5067/CALIOP/CALIPSO/CAL\\_LID\\_L2\\_05kmAPro-Standard-V4-51](https://doi.org/10.5067/CALIOP/CALIPSO/CAL_LID_L2_05kmAPro-Standard-V4-51)). The EAC4 CAMS data is available from (Copernicus Atmosphere Monitoring Service, 2020) (<https://doi.org/10.24381/d58bbf47>). The MISR Plume Height Project 2 data is achieved from software available at <https://iodup05.larc.nasa.gov/merlin/merlin>. The MODIS Collection Active Fire Detections is obtained from (Giglio & Justice, 2021). The necessary code is available via Zenodo (Xu, 2025) (<https://doi.org/10.5281/zenodo.15527018>).

### Acknowledgments

This research is supported by National Key R&D Program of China (2024YFF0809402) (Y.Y.). Computation is supported by High-performance Computing Platform of Peking University.

### References

- Bourgeois, I., Peischl, J., Neuman, J. A., Brown, S. S., Thompson, C. R., Aikin, K. C., et al. (2021). Large contribution of biomass burning emissions to ozone throughout the global remote troposphere. *Proceedings of the National Academy of Sciences of the U S A*, 118(52), e2109628118. <https://doi.org/10.1073/pnas.2109628118>
- Copernicus Atmosphere Monitoring Service. (2020). CAMS global reanalysis (EAC4) [Dataset]. *Copernicus Atmosphere Monitoring Service (CAMS) Atmosphere Data Store*. <https://doi.org/10.24381/d58bbf47>
- Davison, P. S., Roberts, D. L., Arnold, R. T., & Colvile, R. N. (2004). Estimating the direct radiative forcing due to haze from the 1997 forest fires in Indonesia. *Journal of Geophysical Research*, 109(D10). <https://doi.org/10.1029/2003jd004264>
- de Laat, A. T. J., Stein Zweers, D. C., Boers, R., & Tuinder, O. N. E. (2012). A solar escalator: Observational evidence of the self-lifting of smoke and aerosols by absorption of solar radiation in the February 2009 Australian Black Saturday plume. *Journal of Geophysical Research*, 117(D4), D04204. <https://doi.org/10.1029/2011jd017016>
- Dentener, F., Kinne, S., Bond, T., Boucher, O., Cofala, J., Generoso, S., et al. (2006). Emissions of primary aerosol and precursor gases in the years 2000 and 1750 prescribed data-sets for AeroCom. *Atmospheric Chemistry and Physics*, 6(12), 4321–4344. <https://doi.org/10.5194/acp-6-4321-2006>
- Fasullo, J. T., Rosenbloom, N., & Buchholz, R. (2023). A multiyear tropical Pacific cooling response to recent Australian wildfires in CESM2. *Science Advances*, 9(19), eadg1213. <https://doi.org/10.1126/sciadv.adg1213>
- Freitas, S. R., Longo, K. M., Chatfield, R., Latham, D., Dias, M. A. F. S., Andreae, M. O., et al. (2007). Including the sub-grid scale plume rise of vegetation fires in low resolution atmospheric transport models. *Atmospheric Chemistry and Physics*, 7(13), 3385–3398. <https://doi.org/10.5194/acp-7-3385-2007>
- Freitas, S. R., Longo, K. M., Trentmann, J., & Latham, D. (2010). Technical note: Sensitivity of 1-D smoke plume rise models to the inclusion of environmental wind drag. *Atmospheric Chemistry and Physics*, 10(2), 585–594. <https://doi.org/10.5194/acp-10-585-2010>
- Giglio, L., & Justice, C. (2021). MODIS/terra thermal anomalies/fire 5-Min L2 swath 1km V061 [Dataset]. *NASA EOSDIS Land Processes Distributed Active Archive Center DAAC*. <https://doi.org/10.5067/MODIS/MOD14.061>
- Giglio, L., Schroeder, W., & Justice, C. O. (2016). The collection 6 MODIS active fire detection algorithm and fire products. *Remote Sensing of Environment*, 178, 31–41. <https://doi.org/10.1016/j.rse.2016.02.054>
- Gonzalez-Alonso, L., Val Martin, M., & Kahn, R. A. (2019). Biomass-burning smoke heights over the amazon observed from space. *Atmospheric Chemistry and Physics*, 19(3), 1685–1702. <https://doi.org/10.5194/acp-19-1685-2019>
- Hamilton, D. S., Perron, M. M. G., Bond, T. C., Bowie, A. R., Buchholz, R. R., Guieu, C., et al. (2022). Earth, wind, fire, and pollution: Aerosol nutrient sources and impacts on ocean biogeochemistry. *Annual Review of Marine Science*, 14(1), 303–330. <https://doi.org/10.1146/annurev-marine-031921-013612>
- Heinold, B., Baars, H., Barja, B., Christensen, M., Kubin, A., Ohneiser, K., et al. (2022). Important role of stratospheric injection height for the distribution and radiative forcing of smoke aerosol from the 2019–2020 Australian wildfires. *Atmospheric Chemistry and Physics*, 22(15), 9969–9985. <https://doi.org/10.5194/acp-22-9969-2022>
- Hersbach, H., Bell, B., Berrisford, P., Biavati, G., Horányi, A., Muñoz Sabater, J., et al. (2023a). ERA5 hourly data on pressure levels from 1940 to present [Dataset]. *Copernicus Climate Change Service (C3S) Climate Data Store (CDS)*. <https://doi.org/10.24381/cds.bd0915c6>
- Hersbach, H., Bell, B., Berrisford, P., Biavati, G., Horányi, A., Muñoz Sabater, J., et al. (2023b). ERA5 hourly data on single levels from 1940 to present [Dataset]. *Copernicus Climate Change Service (C3S) Climate Data Store (CDS)*. <https://doi.org/10.24381/cds.adbb2d47>

- Huang, J., Loría-Salazar, S. M., Deng, M., Lee, J., & Holmes, H. A. (2024). Assessment of smoke plume height products derived from multisource satellite observations using lidar-derived height metrics for wildfires in the Western US. *Atmospheric Chemistry and Physics*, 24(6), 3673–3698. <https://doi.org/10.5194/acp-24-3673-2024>
- Inness, A., Ades, M., Agustí-Panareda, A., Barré, J., Benedictow, A., Blechschmidt, A. M., et al. (2019). The CAMS reanalysis of atmospheric composition. *Atmospheric Chemistry and Physics*, 19(6), 3515–3556. <https://doi.org/10.5194/acp-19-3515-2019>
- Janssen, T. A. J., Jones, M. W., Finney, D., van der Werf, G. R., van Wees, D., Xu, W., & Veraverbeke, S. (2023). Extratropical forests increasingly at risk due to lightning fires. *Nature Geoscience*, 16(12), 1136–1144. <https://doi.org/10.1038/s41561-023-01322-z>
- Kahn, R. A., Li, W. H., Moroney, C., Diner, D. J., Martonchik, J. V., & Fishbein, E. (2007). Aerosol source plume physical characteristics from space-based multiangle imaging. *Journal of Geophysical Research*, 112(D11), D11205. <https://doi.org/10.1029/2006jd007647>
- Kaiser, J. W., Heil, A., Andreae, M. O., Benedetti, A., Chubarova, N., Jones, L., et al. (2012). Biomass burning emissions estimated with a global fire assimilation system based on observed fire radiative power. *Biogeosciences*, 9(1), 527–554. <https://doi.org/10.5194/bg-9-527-2012>
- Khaykin, S., Legras, B., Bucci, S., Sellitto, P., Isaksen, I., Tencé, F., et al. (2020). The 2019/20 Australian wildfires generated a persistent smoke-charged vortex rising up to 35 km altitude. *Communications Earth & Environment*, 1(1), 22. <https://doi.org/10.1038/s43247-020-00022-5>
- Kim, M. H., Omar, A. H., Tackett, J. L., Vaughan, M. A., Winker, D. M., Trepte, C. R., et al. (2018). The CALIPSO version 4 automated aerosol classification and lidar ratio selection algorithm. *Atmospheric Measurement Techniques*, 11(11), 6107–6135. <https://doi.org/10.5194/amt-11-6107-2018>
- Koning, H. W. D., Smith, K. R., & Last, J. M. (1985). Biomass fuel combustion and health. *Bulletin of the World Health Organization*, 63(1), 11–26.
- Labonne, M., Bréon, F. M., & Chevallier, F. (2007). Injection height of biomass burning aerosols as seen from a spaceborne lidar. *Geophysical Research Letters*, 34(11), L11806. <https://doi.org/10.1029/2007gl029311>
- Li, M., Shen, F., & Sun, X. (2021). 2019–2020 Australian bushfire air particulate pollution and impact on the south Pacific Ocean. *Scientific Reports*, 11(1), 12288. <https://doi.org/10.1038/s41598-021-91547-y>
- Li, Y., Tong, D., Ma, S., Freitas, S. R., Ahmadov, R., Sofiev, M., et al. (2023). Impacts of estimated plume rise on PM<sub>2.5</sub> exceedance prediction during extreme wildfire events: A comparison of three schemes (Briggs, Freitas, and Sofiev). *Atmospheric Chemistry and Physics*, 23(5), 3083–3101. <https://doi.org/10.5194/acp-23-3083-2023>
- Lu, Z., Liu, X., Ke, Z., Zhang, K., Ma, P. L., & Fan, J. (2023). Incorporating an interactive fire plume-rise model in the doe's energy exascale Earth system model version 1 (E3SMv1) and examining aerosol radiative effect. *Journal of Advances in Modeling Earth Systems*, 16(1), e2023MS003818. <https://doi.org/10.1029/2023ms003818>
- Ma, C., Ni, R., Su, H., & Cheng, Y. (2024). Enhancing global simulation of smoke injection height for intense pyro-convection through coupling an improved one-dimensional plume rise model in CAM-chem. *Journal of Advances in Modeling Earth Systems*, 16(10), e2023MS004127. <https://doi.org/10.1029/2023ms004127>
- Meng, X., Yu, Y., & Ginoux, P. (2025). Rise in dust emissions from burned landscapes primarily driven by small fires. *Nature Geoscience*, 18(7), 586–592. <https://doi.org/10.1038/s41561-025-01730-3>
- Michailidis, K., Koukoulis, M.-E., Siomos, N., Balis, D., Tuinder, O., Tilstra, L. G., et al. (2021). First validation of GOME-2/MetOp absorbing aerosol height using EARLINET lidar observations. *Atmospheric Chemistry and Physics*, 21(4), 3193–3213. <https://doi.org/10.5194/acp-21-3193-2021>
- NASA/LARC/SD/ASDC. (2022b). CALIPSO lidar level 2 vertical feature mask (VFM) [Dataset]. *NASA Langley Atmospheric Science Data Center DAAC*, V4–51. [https://doi.org/10.5067/CALIPSO/CALIPSO/CAL\\_LID\\_L2\\_VFM-Standard-V4-51](https://doi.org/10.5067/CALIPSO/CALIPSO/CAL_LID_L2_VFM-Standard-V4-51)
- NASA/LARC/SD/ASDC. (2022a). CALIPSO lidar level 2 aerosol profile, V4-51 [Dataset]. *NASA Langley Atmospheric Science Data Center DAAC*. [https://doi.org/10.5067/CALIPSO/CALIPSO/CAL\\_LID\\_L2\\_05kmAPro-Standard-V4-51](https://doi.org/10.5067/CALIPSO/CALIPSO/CAL_LID_L2_05kmAPro-Standard-V4-51)
- Nelson, D., Garay, M., Kahn, R., & Dunst, B. (2013). Stereoscopic height and wind retrievals for aerosol plumes with the MISR Interactive Explorer (MINX). *Remote Sensing*, 5(9), 4593–4628. <https://doi.org/10.3390/rs5094593>
- Ohneiser, K., Ansmann, A., Witthuhn, J., Deneke, H., Chudnovsky, A., Walter, G., & Senf, F. (2023). Self-lofting of wildfire smoke in the troposphere and stratosphere: Simulations and space lidar observations. *Atmospheric Chemistry and Physics*, 23(4), 2901–2925. <https://doi.org/10.5194/acp-23-2901-2023>
- Paugam, R., Wooster, M., Freitas, S., & Val Martin, M. (2016). A review of approaches to estimate wildfire plume injection height within large-scale atmospheric chemical transport models. *Atmospheric Chemistry and Physics*, 16(2), 907–925. <https://doi.org/10.5194/acp-16-907-2016>
- Peterson, D. A., Campbell, J. R., Hyer, E. J., Fromm, M. D., Kablick, G. P., Cossuth, J. H., & DeLand, M. T. (2018). Wildfire-driven thunderstorms cause a volcano-like stratospheric injection of smoke. *npj Climate and Atmospheric Science*, 1, 30. <https://doi.org/10.1038/s41612-018-0039-3>
- Peterson, D. A., Fromm, M. D., McRae, R. H. D., Campbell, J. R., Hyer, E. J., Taha, G., et al. (2021). Australia's Black Summer pyrocumulonimbus super outbreak reveals potential for increasingly extreme stratospheric smoke events. *npj Climate and Atmospheric Science*, 4(1), 38. <https://doi.org/10.1038/s41612-021-00192-9>
- Powell, K. A., Hu, Y., Omar, A., Vaughan, M. A., Winker, D. M., Liu, Z., et al. (2009). Overview of the CALIPSO mission and CALIOP data processing algorithms. *Journal of Atmospheric and Oceanic Technology*, 26(11), 2310–2323. <https://doi.org/10.1175/2009jtecha1281.1>
- Rodríguez, B., Lareau, N. P., Kingsmill, D. E., & Clements, C. B. (2020). Extreme pyroconvective updrafts during a megafire. *Geophysical Research Letters*, 47(18), e2020GL089001. <https://doi.org/10.1029/2020gl089001>
- Rosenfeld, D., Fromm, M., Trentmann, J., Luderer, G., Andreae, M. O., & Servranckx, R. (2007). The chisholm firestorm: Observed microstructure, precipitation and lightning activity of a pyro-cumulonimbus. *Atmospheric Chemistry and Physics*, 7(3), 645–659. <https://doi.org/10.5194/acp-7-645-2007>
- Sofiev, M., Ermakova, T., & Vankevich, R. (2012). Evaluation of the smoke-injection height from wild-land fires using remote-sensing data. *Atmospheric Chemistry and Physics*, 12(4), 1995–2006. <https://doi.org/10.5194/acp-12-1995-2012>
- Sofiev, M., Vankevich, R., Ermakova, T., & Hakkarainen, J. (2013). Global mapping of maximum emission heights and resulting vertical profiles of wildfire emissions. *Atmospheric Chemistry and Physics*, 13(14), 7039–7052. <https://doi.org/10.5194/acp-13-7039-2013>
- Su, H., Yu, Y., Guo, W., & Mao, J. (2025). Convective potential and fuel availability complement near-surface weather in regulating global wildfire activity. *Science Advances*, 11(8), eadp7765. <https://doi.org/10.1126/sciadv.adp7765>
- Tosca, M. G., Randerson, J. T., Zender, C. S., Nelson, D. L., Diner, D. J., & Logan, J. A. (2011). Dynamics of fire plumes and smoke clouds associated with peat and deforestation fires in Indonesia. *Journal of Geophysical Research*, 116(D8), D08207. <https://doi.org/10.1029/2010jd015148>
- Val Martin, M., Kahn, R., & Tosca, M. (2018). A global analysis of wildfire smoke injection heights derived from space-based multi-angle imaging. *Remote Sensing*, 10(10), 1609. <https://doi.org/10.3390/rs10101609>

- Val Martin, M., Logan, J. A., Kahn, R. A., Leung, F. Y., Nelson, D. L., & Diner, D. J. (2010). Smoke injection heights from fires in North America: Analysis of 5 years of satellite observations. *Atmospheric Chemistry and Physics*, *10*(4), 1491–1510. <https://doi.org/10.5194/acp-10-1491-2010>
- Veira, A., Kloster, S., Wilkenskield, S., & Remy, S. (2015). Fire emission heights in the climate system – Part 1: Global plume height patterns simulated by ECHAM6-HAM2. *Atmospheric Chemistry and Physics*, *15*(13), 7155–7171. <https://doi.org/10.5194/acp-15-7155-2015>
- Westphal, D. L., & Toon, O. B. (2012). Simulations of microphysical, radiative, and dynamical processes in a continental-scale forest fire smoke plume. *Journal of Geophysical Research*, *96*(D12), 22379–22400. <https://doi.org/10.1029/91jd01956>
- Xu, R. (2025). XuRui1204/Two-step-smoke-plume-height-model: Atmospheric convection and aerosol absorption boost wildfire smoke injection (wildfire) [Software]. *Zenodo*. <https://doi.org/10.5281/zenodo.15527018>
- Yu, P., Toon, O. B., Bardeen, C. G., Zhu, Y., Rosenlof, K. H., Portmann, R. W., et al. (2019). Black carbon lofts wildfire smoke high into the stratosphere to form a persistent plume. *Science*, *365*(6453), 587–590. <https://doi.org/10.1126/science.aax1748>
- Zhang, Y., Fan, J., Logan, T., Li, Z., & Homeyer, C. R. (2019). Wildfire impact on environmental thermodynamics and severe convective storms. *Geophysical Research Letters*, *46*(16), 10082–10093. <https://doi.org/10.1029/2019gl084534>